Journal of Solid State Chemistry 183 (2010) 1442–1447

Contents lists available at ScienceDirect

Journal of Solid State Chemistry

journal homepage: www.elsevier.com/locate/jssc

Solid state synthesis of water-dispersible silicon nanoparticles from silica nanoparticles

Keren Kravitz [a], Alexander Kamyshny [a,*], Aharon Gedanken [b], Shlomo Magdassi [a]

[a] Casali Institute of Applied Chemistry, Institute of Chemistry, The Hebrew University of Jerusalem, Jerusalem 91904, Israel
[b] Department of Chemistry and Kanbar Laboratory for Nanomaterials, Bar-Ilan University Center for Advanced Materials and Nanotechnology, Bar-Ilan University, Ramat-Gan 52900, Israel

ARTICLE INFO

Article history:
Received 31 January 2010
Received in revised form
13 April 2010
Accepted 14 April 2010
Available online 21 April 2010

Keywords:
Nanoparticles
Silicon nanoparticles
Silicon photoluminescence
Stabilization of nanoparticles

ABSTRACT

A solid state synthesis for obtaining nanocrystalline silicon was performed by high temperature reduction of commercial amorphous nanosilica with magnesium powder. The obtained silicon powder contains crystalline silicon phase with lattice spacings characteristic of diamond cubic structure (according to high resolution TEM), and an amorphous phase. In ^{29}Si CP MAS NMR a broad multicomponent peak corresponding to silicon is located at −61.28 to −69.45 ppm, i.e. between the peaks characteristic of amorphous and crystalline Si. The powder has displayed red luminescence while excited under UV illumination, due to quantum confinement within the nanocrystals. The silicon nanopowder was successfully dispersed in water containing poly(vinyl alcohol) as a stabilizing agent. The obtained dispersion was also characterized by red photoluminescence with a band maximum at 710 nm, thus enabling future functional coating applications.

1. Introduction

Since Canham's discovery of red photoluminescence (PL) from porous silicon at room temperature [1], the interest in various forms of nanostructured silicon is continuously growing.

Bulk silicon is indirect band-gap (1.12 eV) semiconductor, in which the optical transitions are allowed only if phonons are absorbed or emitted to conserve the crystal momentum. It is therefore an inefficient emitter, even at low temperatures. However, in the nanometric size range the fundamental properties of silicon nanoparticles (Si NPs) differ from those of bulk material due to the quantum confinement effect: when the electron–hole pair (exciton), is created after photon irradiation, it is confined within the crystallites (exciton radius for silicon is 4.3 nm [2]). The spatial reduction of dimensions to nanosize range increases the uncertainty in the exciton momentum, thus increasing the probability of band to band recombination accompanied by photon emission [3–5].

Since silicon is an abundant, nontoxic, biocompatible, environmental friendly and low cost material, silicon nanoparticles are promising material for fabrication of novel devices such as light sources (lasers, light-emitting diodes), photovoltaic cells [3,5–7], memory devices [8] and can be also used as luminescent probes for bioimaging [5,9].

There are two main approaches to synthesize silicon nanoparticles: "top down" based on high-energy dispersing of bulk material, and "bottom-up" based on formation of nanoparticles from precursor molecules. The "bottom up" fabrication of silicon nanoparticles can be performed by three main routes: gas phase, solution and solid state. Gas phase processes, e.g. high energy decomposition of silane, like top down methods, yield usually particles with broad size distribution [10,11] and rapid agglomeration, since the formed particles are not charged and are not protected against aggregation by proper capping agents. The solution phase processes allow capping of nanoparticles at early stages of their formation, thus preventing aggregation that results in rather narrow particles size distribution. However, preparation of silicon nanoparticles by these routes is characterized by rather low yields [12,13].

Three main approaches to solid state synthesis of silicon nanoparticles were reported: reaction of polyanionic "Zintl" phases (e.g. NaSi) with metal halides at 200–500 °C in a glove box [14], rapid metathesis reaction of sodium silicofluoride (Na_2SiF_6) with sodium azide (NaN_3) at 950–1000 °C [15], and reduction of silica (400–650 nm) and Mediterranean sand with magnesium by reaction under autogenic pressure at elevated temperature (RAPET) [16]. In addition, silicon nanocrystals were obtained as a by-product while preparing magnesia from silica-based *Aulacoseira* diatom frustules by reduction with magnesium vapor [17].

In this paper, we present a simple solid state process for synthesis of photoluminescent silicon nanocrystals with the use

* Corresponding author. Fax: +972 2 6584350.
E-mail address: kamyshny@vms.huji.ac.il (A. Kamyshny).

0022-4596/$ - see front matter © 2010 Elsevier Inc. All rights reserved.
doi:10.1016/j.jssc.2010.04.023

of a low cost commercial precursor, which is an aqueous dispersion of amorphous silica nanoparticles. The process is based on high temperature reduction of the silica nanoparticles with magnesium powder. The effect of the reaction conditions (temperature and reaction duration) on the crystallinity of the obtained nanoparticles was evaluated. The preparation of photoluminescent dispersions of obtained silicon nanoparticles, which can be used for surfaces coating is also presented.

2. Experimental

2.1. Materials

Aqueous dispersion of amorphous silica nanoparticles (Ludox HS®, 40 wt%, average particle size 11.5 nm) poly(vinyl alcohol) (PVA), MW 13,000–23,000 and gelatin (type B approx. 75 Bloom), were purchased from Sigma-Aldrich, and Mg powder (≥99%) was purchased form Fluka. All other reagents were of analytical grade.

2.2. Synthesis

Magnesium powder (0.65 g) was added to 2 g of 0.5 wt% aqueous gelatin solution containing 0.2 g of silica dispersion (SiO_2:Mg molar ratio of 1:20), the mixture was immediately frozen in a liquid N_2 bath and lyophilized overnight. The gelatin was used to obtain a homogenous powder after lyophilization. The obtained powder was placed in a ceramic crucible, and heated in a tube furnace for 5 h at the required temperature, 520–750 °C under N_2 (the temperature was raised at a rate of 10 °C/min). The sample was collected after cooling the reaction mixture at room temperature. All the by-products were removed by treatment with a concentrated hydrochloric acid (37 wt%) for 24 h. The obtained product was then washed three times with distilled water and dried at room temperature overnight. The reaction yield (wt%) was calculated as the ratio of obtained crystalline silicon to the theoretical according the reaction scheme.

2.3. Dispersion preparation

Dispersions of silicon nanoparticles (0.1 wt%) were prepared by mixing silicon powder in aqueous solution of PVA as a stabilizing agent (0.05 wt%) in ultrasonic bath (B-1510, Bransonic) for 5 min followed by wet-milling for 2 h at 5000 rpm in Dispermat (Dispermat-CV, VMA-Getzmann GmbH, Germany) with the use of 0.3 μm zirconia beads.

2.4. Characterization methods

X-ray powder diffraction measurements were performed by using D8 Advance diffractometer (Bruker AXS, Karlsruhe, Germany) with a goniometer radius of 217.5 mm, Göbel mirror parallel-beam optics, 2° Sollers slits and 0.2 mm receiving slit. The crystallite size was calculated from the XRD data by the Scherrer equation [18]:

$$L = \frac{\kappa\lambda}{\beta * \cos\theta} \quad (1)$$

where K is Scherrer constant ($0.89 < K < 1$), λ is the X-ray wavelength, β is the full-width at half-maximum (FWHM) of the peaks and θ is the Bragg angle.

The degree of crystallinity of the powders was calculated using the following relation:

$$DC = \frac{s_{cr}}{s_{cr} + s_{am}} \times 100\% \quad (2)$$

where S_{cr} is the total area of peaks of the crystalline phase and S_{am} is the area of the "halo" from the amorphous phase [19].

Particles size in the dispersions was measured by dynamic light scattering (DLS), using Nano-ZS Zetasizer (Malvern, UK), which detects particles in a size range of 0.6 nm–6 μm. The measurements were performed twice and the size distributions were presented as number distributions.

HR-TEM imaging was performed with FEI Technai F20G^2 operating at 200 keV accelerating voltage. Samples were prepared by dispersing the silicon powder in ethanol in ultrasonic bath and placing a drop of the obtained dispersion on a carbon coated copper grid followed by drying in vacuum.

HR-SEM imaging was performed with FEI Sirion HR-SEM (accelerating voltages from 200 V to 30 kV) equipped with EDS microanalyzer.

Zeta potential measurements were performed at 25 °C with Nano-ZS Zetasizer (Malvern, UK). The samples before measurements were diluted with 10 mM NaCl solution.

Solid state ^{29}Si CPMAS NMR spectrum was recorded with a Bruker AVANCE II 500 NMR spectrometer using a broadband 4 mm probe. The spectra were measured at a Larmor frequency of 99.38 MHz and spinning speed of 12 kHz. Spectrum pulse lengths of 2.8 μs were used at a B_1 field of 83 kHz for both ^{29}Si and ^{1}H, the recycling delay was 10 s. The chemical shift was externally referenced to ^{13}C-adamantane (ratio $\nu_0(^{13}C)$ $\Xi(^{29}Si)/\Xi(^{13}C) = \nu_0(^{29}Si)$, $\Xi(^{13}C) = 0.25145020$, $\Xi(^{29}Si) = 0.19867187$).

Photoluminescence spectra of the dispersions were measured with a Varian Cary Eclipse spectrofluorimeter.

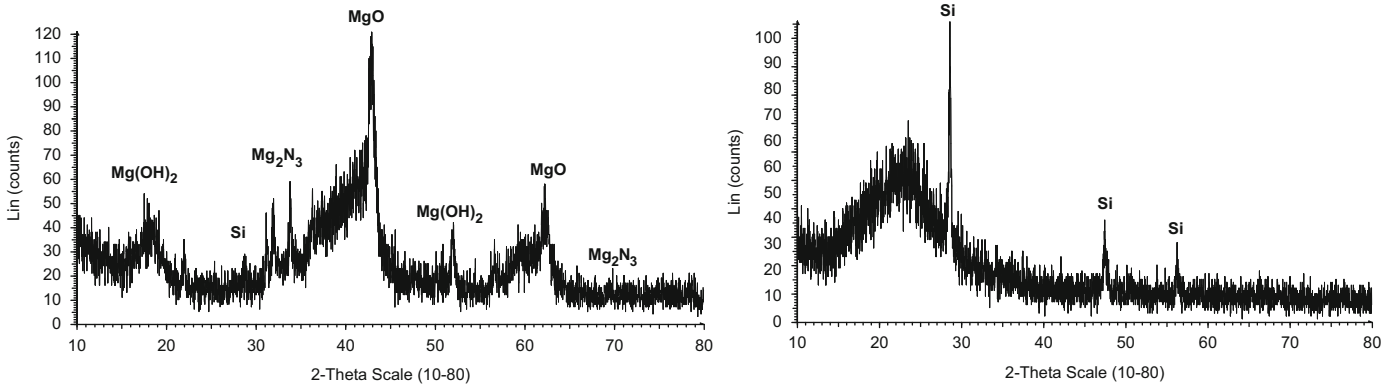

Fig. 1. XRD pattern of the powder before treatment with HCl (a) and after removal of the reaction by-products by HCl (b).

3. Results and discussion

3.1. Synthesis

The synthesis of silicon nanoparticles was performed at SiO_2:Mg molar ratio of 1:20, since at lower ratios no photoluminescence of the obtained powder was detected. Typical synthesis of silicon nanoparticles was carried out at 750 °C. The reaction proceeds according to the following scheme:

$$SiO_2 + 2Mg \rightarrow Si + 2MgO \quad (3)$$

Because of the excess of magnesium in the reaction mixture, in addition to the silicon and magnesium oxide, magnesium nitride as by-product (synthesis was performed in N_2 atmosphere) was formed according to reaction 4:

$$3Mg + N_2 \rightarrow Mg_3N_2 \quad (4)$$

This byproduct was detected in the XRD of the reaction product (Fig. 1a).

The presence of minor amounts of magnesium hydroxide is a result of post-reaction hydration of MgO after exposure of the powder to air.

In order to remove the byproducts, the obtained powders were treated with concentrated HCl at room temperature followed by thorough washing with triply distilled water and drying at ambient conditions. The HCl treatment and washing are accompanied by the following reactions (Eq. 6 [20]):

$$MgO + 2HCl \rightarrow MgCl_2 + H_2O \quad (5)$$

$$Mg_3N_2 + 6H_2O \rightarrow 3Mg(OH)_2 + 2NH_3 \quad (6)$$

$$Mg(OH)_2 + 2HCl \rightarrow MgCl_2 + 2H_2O \quad (7)$$

The products formed in reaction with aqueous HCl are water soluble ($MgCl_2$). The final product after thorough washing with triply distilled water was obtained as a gray powder, which was further characterized as described below. The yield of crystalline silicon was calculated to be 18%.

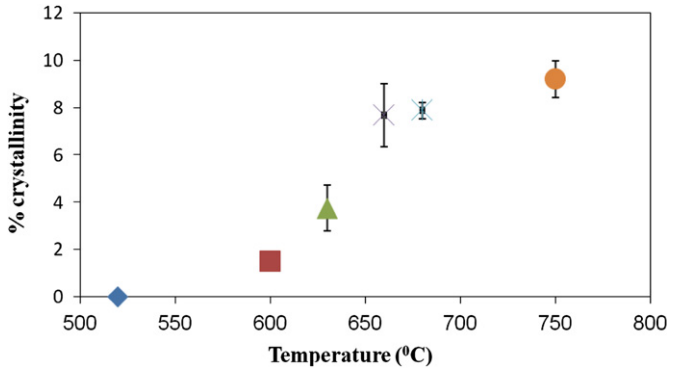

Fig. 2. Degree of the powder crystallinity as a function of the reaction temperature.

3.2. Characterization of powders

Fig. 1b shows the XRD pattern of washed and dried powder. Only peaks corresponding to crystalline silicon were detected, the average degree of weight crystallinity of the powders and the average crystallite size were $11 \pm 6\%$ and 43 ± 10 nm (according to the Scherrer equation), respectively. The "halo" in the XRD pattern is a result of the presence of a large amount of amorphous phase in the obtained powder.

To evaluate the effect of the reaction temperature on the crystallinity of the silicon nanocrystals, the reaction was performed at 520°, 600°, 630°, 660°, 680° and 750 °C for 1 h, while the SiO_2:Mg ratio was kept constant, 1:20. The degree of the powder crystallinity as a function of the reaction temperature is presented in Fig. 2. It was found that no crystalline phase was formed at 520 °C. At 600 °C, a crystalline phase was detected, but the degree of crystallinity was very low, and calculation of particles size from this XRD data could not be performed. At temperatures from 630 °C up to 750 °C (m.p. of Mg is 650 °C), the crystalline phase was obtained with negligible change in crystallites size while changing the temperature. The average crystallite size was found to be 39 ± 6 nm.

The effect of reaction duration on the characteristics of obtained material has been also evaluated. There was no noticeable difference in the crystallite size or in the degree of crystallinity while performing the reaction for 0.5, 1, 2, 3 and 5 h.

As seen from the HR-SEM image of the sample prepared at 750 °C for 5 h (Fig. 3a), the powder is composed of agglomerated nanoparticles. According to quantitative EDS analysis (Fig. 3b), the main element in the powder is silicon (~75 at%), but rather large amount of oxygen (~20 at%) indicates that a part of the material is silicon oxide (atomic Si:O ratio is ~3.85).

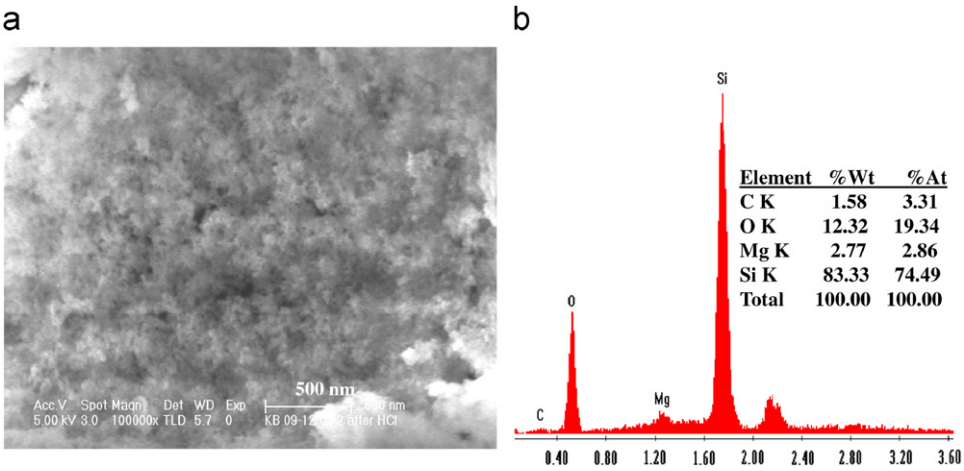

Fig. 3. HR-SEM image of the powder prepared at 750 °C for 5 h (a) and EDS with the results of microanalysis (b).

Fig. 4 shows the solid state ^{29}Si CP MAS NMR pattern of Si powder with ~10% of crystallinity. The position of broad multicomponent peak at −61.28 to −69.45 ppm corresponding to elemental Si is between the peaks characteristic of amorphous and crystalline Si (approximately 50 and 80 ppm, respectively) [21–24]. The signal with peaks at −101.32 and −110.99 ppm can be attributed to the presence of Si–O bonds at the surface of nanoparticles (O–Si–O, Si–OH) [22,23,25].

The powder that was prepared at 750 °C and 5 h duration has been also characterized by HR-TEM (Fig. 5). Crystal lattice is clearly seen, and the lattice spacings of 0.317, 0.196 and 0.167 nm matches, respectively, the (1,1,1), (2,2,0) and (3,1,1) planes of diamond cubic structured silicon. The HR-TEM images clearly indicate the presence of much smaller crystals (4–10 nm) as compared with estimation made with the use of Scherrer equation (~40 nm). These nanocrystals are apparently embedded within an amorphous matrix. The discrepancy in size determination is not unusual since the particle size distribution is wide, and the Scherrer equation gives the mean crystallite size [26].

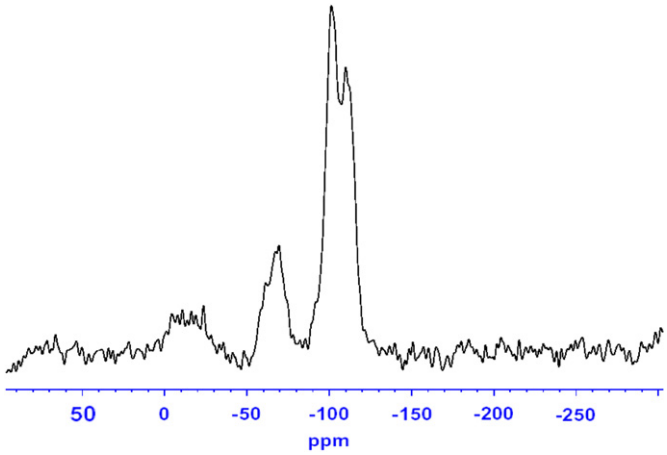

Fig. 4. ^{29}Si CP MAS NMR spectrum of powder with 10% degree of crystallinity.

While exciting the powder under UV light, a strong red emission was observed. In order to relate the particle size to the bandgap energy of the quantum dot and to the PL wavelength, an effective mass model has been applied. According to this model [5], red emission of silicon quantum dots is expected in the size range of 2.5–3 nm. The detection of red PL indicates that the powder does contain silicon nanoparticles in this size range, which is smaller than the calculated according to the Scherrer equation. The possibility that specific surface sites contribute to the visible PL of silicon nanoparticles by formation of localized levels in bandgap also cannot be excluded [27]. Such localized levels can be provided by formation of surface Si=O or Si–OH bonds [2,28–30].

3.3. Preparation and characterization of dispersions

Stable dispersions of silicon nanoparticles are required for preparation of formulations, which can be used for coating of various surfaces. Aqueous dispersions of silicon nanocrystals were obtained by mixing the silicon powder in aqueous solutions of polymeric stabilizing agents in an ultrasonic bath, followed by wet-milling in the presence of 0.3 μm zirconia beads.

After evaluation of various polymeric agents in order to find those with good dispersing and stabilizing efficiency and negligible emission in the visible range, PVA with MW in the range of 13,000–23,000 was selected. The silicon nanoparticles showed good dispersibility in water in the presence of this polymeric stabilizer. The particle size distribution of the obtained dispersion according to DLS is shown in Fig. 6. The average particle size was found to be 101 ± 6 nm (by number distribution). In view of the previous results, it can be assumed that these particles are composed of aggregates of nanocrystals and amorphous material.

Fig. 7 shows the zeta potential as a function of pH. As the pH increases, the zeta potential of the dispersion changes from about

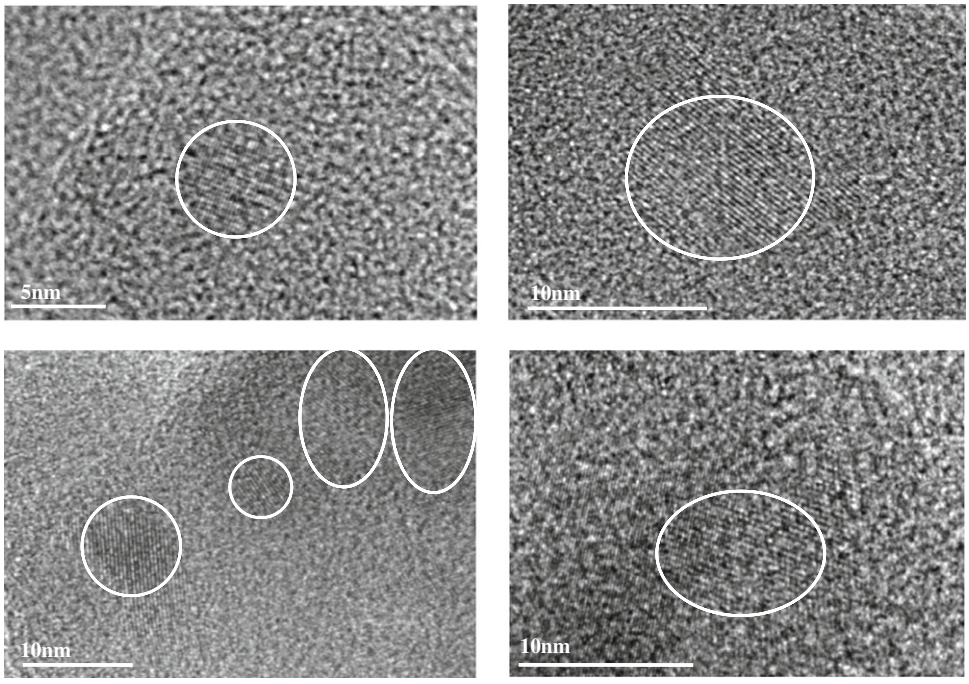

Fig. 5. HR-TEM image of Si nanocrystals in powder prepared at 750 °C for 5 h.

+2 mV at pH 1.3 to about −28 mV at pH 7 with a wide plateau in the pH range from 6.5 to 12. Since PVA is a nonionic polymeric stabilizer, the negative charge can be a result of the ionization of surface silanol groups of partially oxidized silicon nanoparticles [31]. The presence of silanol groups is expected, in view of the presence of oxygen in the powder and the NMR results.

Like silicon nanoparticles in powder, the silicon nanoparticles in aqueous dispersion (pH 7.7) also display red PL under UV excitation (320 nm) (Fig. 8). The PL spectrum is characterized by broad band with maximum at 710 nm and shoulder at 820 nm that corresponds, according to calculations based on the effective mass model to crystals in the size range of 2.5–3 nm.

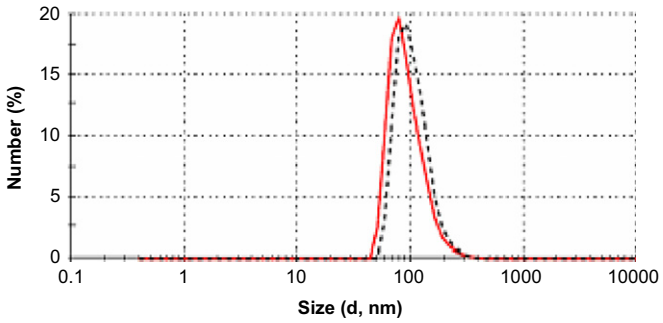

Fig. 6. Size distribution of silicon nanoparticles in aqueous dispersion by DLS (2 runs, number distribution).

4. Conclusions

Silicon nanocrystals were successfully synthesized by simple solid state method—reduction of commercial amorphous nano-silica by magnesium at high temperature. The obtained silicon powder was composed of nanocrystals of diamond cubic structure embedded in amorphous matrix and was characterized by red PL while excited with UV light. Stable aqueous dispersion of silicon nanoparticles was prepared with the use of PVA as a stabilizing agent. The obtained dispersion was also characterized by red photoluminescence with a band maximum at 710 nm, the origin of which is supposed to be quantum confinement effect. Such dispersions may be promising precursors for development of formulations, which can be used for silicon coating of various substrates by, for example, ink-jet printing that paves the way for fabrication of optoelectronic devices, e.g. light sources (lasers and light-emitting diodes) and photovoltaic cells.

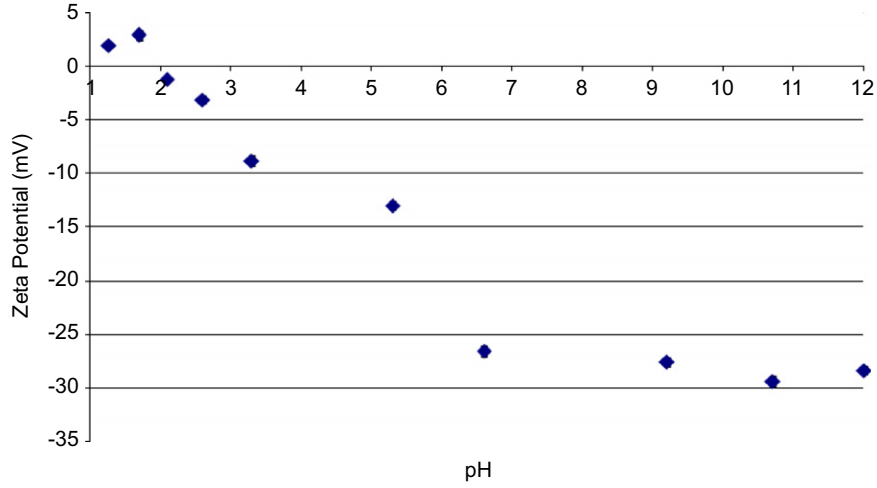

Fig. 7. Zeta potential of Si nanoparticles in aqueous dispersion stabilized by PVA as a function of pH.

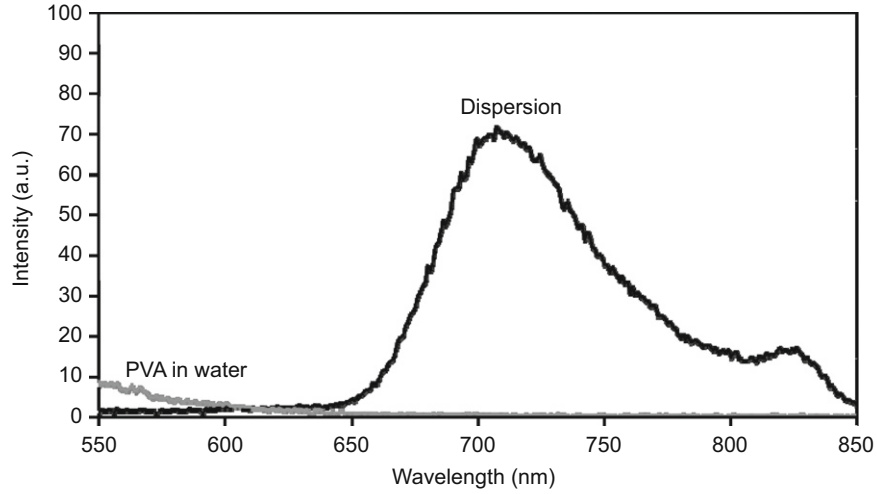

Fig. 8. PL spectrum of the aqueous dispersion of Si nanoparticles (lower curve is luminescence of control sample—aqueous solution of PVA). Excitation wavelength is 320 nm.

References

[1] L.T. Canham, Appl. Phys. Lett. 57 (1990) 1046–1048.
[2] S.W. Lin, D.H. Chen, Small 5 (2009) 72–76.
[3] C.J. Murphy, J.L. Coffer, Appl. Spectrosc. 56 (2002) 16a–27a.
[4] A.D. Yoffe, Adv. Phys. 50 (2001) 1–208.
[5] M.H. Nayfeh, L. Mitas, Silicon nanoparticles: new photonic and electronic material at the transition between solid and molecule, in: V. Kumar (Ed.), Nanosilicon, Elsevier, Amsterdam, Oxford, 2008, pp. 1–78.
[6] M. Stupca, M. Alsalhi, T. Al Saud, A. Almuhanna, M.H. Nayfeh, Appl. Phys. Lett. 91 (2007) 063107-1–063107-3.
[7] V. Svrcek, A. Slaoui, J.C. Muller, Thin Solid Films 451–52 (2004) 384–388.
[8] S. Tiwari, F. Rana, H. Hanafi, A. Hartstein, E.F. Crabbe, K. Chan, Appl. Phys. Lett. 68 (1996) 1377–1379.
[9] J. Choi, N.S. Wang, V. Reipa, Bioconjugate Chem. 19 (2008) 680–685.
[10] A. Gupta, M.T. Swihart, H. Wiggers, Adv. Funct. Mater. 19 (2009) 696–703.
[11] M.L. Ostraat, H.A. Atwater, R.C. Flagan, J. Colloid Interface Sci. 283 (2005) 414–421.
[12] J.R. Heath, Science 258 (5085) (1992) 1131–1133.
[13] J. Zou, P. Sanelle, K.A. Pettigrew, S.M. Kauzlarich, J. Cluster Sci. 17 (2006) 565–578.
[14] P.F. McMillan, J. Gryko, C. Bull, R. Arledge, A.J. Kenyon, B.A. Cressey, J. Solid State Chem. 178 (2005) 937–949.
[15] C.W. Won, H.H. Nersisyan, H.I. Won, H.H. Lee, J. Solid State Chem. 182 (2009) 3201–3206.
[16] N.H. Hai, I. Grigoriants, A. Gedanken, J. Phys. Chem. C 113 (2009) 10521–10526.
[17] Y. Cai, S.M. Allan, K.H. Sandhage, J. Am. Ceram. Soc. 88 (2005) 2005–2010.
[18] B.D. Cullity, Elements of X-ray Diffraction, second ed, Addison Wesley, Reading, MA, 1978.
[19] W. Shujun, Y. Jinglin, G. Wenyuan, Am. J. Biochem. Biotechnol. 1 (2005) 199–203.
[20] J.Q. Hu, Y. Bando, J.H. Zhan, C.Y. Zhi, D. Goldberg, Nano Lett. 6 (2006) 1136–1140.
[21] D. Mayeri, B.L. Phillips, M.P. Augustine, S.M. Kauzlarich, Chem. Mater. 13 (2001) 765–770.
[22] W.K. Chang, M.Y. Liao, K.K. Gleason, J. Phys. Chem. 100 (1996) 19653–19658.
[23] J.S. Hartman, M.F. Richardson, B.L. Sherriff, B.G. Winsborrow, J. Am. Chem. Soc. 109 (1987) 6059–6067.
[24] W.L. Shao, J. Shinar, B.C. Gerstein, F. Li, J.S. Lannin, Phys. Rev. B 41 (1990) 9491–9494.
[25] M.L. Balmer, B.C. Bunker, L.Q. Wang, C.H.F. Peden, Y.L. Su, J. Phys. Chem. B 101 (1997) 9170–9179.
[26] V. Uvarov, I. Popov, Mater. Charact. 58 (2007) 883–891.
[27] M.V. Wolkin, J. Jorne, P.M. Fauchet, G. Allan C. Delerue, Phys. Rev. Lett. 82 (1999) 197–200.
[28] F.J. Hua, F. Erogbogbo, M.T. Swihart, E. Ruckenstein, Langmuir 22 (2006) 4363–4370.
[29] A. Sáar, Y. Reichman, M. Dovrat, D. Krapf, J. Jedrzejewski, I. Balberg, Nano Lett. 5 (2005) 2443–2447.
[30] L. Tsybeskov, J.V. Vandyshev, P.M. Fauchet, Phys. Rev. B 49 (1994) 7821–7824.
[31] M. Kosmulski, J. Colloid Interface Sci. 275 (2004) 214–224.